The Role of Radiation in Common Envelope Evolution

Logan J. Prust[*]
Department of Physics, University of Wisconsin-Milwaukee
Milwaukee, WI, USA

Abstract

The common envelope phase in binary star systems is simulated using the 3-D moving-mesh hydrodynamic code MANGA. The radiation hydrodynamics module in MANGA is modified using a sub-cycling algorithm to skip unnecessary calculations. The sub-cycling as well as other optimizations reduce computation time by a factor of 3. The generation of appropriate initial conditions for radiation hydrodynamic simulations is discussed.

1. Introduction

Common envelope evolution (CEE) is a phase during the life of a binary star system in which a giant star shares its gaseous envelope with a smaller companion object: a small star or a stellar remnant (for a review see Ivanova et al. 2013). The transfer of orbital energy and angular momentum from the giant's core and companion to the gas drives partial or complete ejection of the envelope from the system. This, in turn, causes the separation between the core and companion to decrease. This process is important for the formation of X-ray binaries, double white dwarfs, and double neutron stars, and may also be responsible for the merging black hole systems observed by Advanced LIGO (Ivanova et al. 2013). Despite its importance, CEE is not well understood, and this is due in part to the number of different physics that must be included as well as the range of time-scales involved. Furthermore, there is uncertainty as to whether the contributions from recombination and radiation energy should be included. Because of these challenges, our current understanding of CEE is limited at best.

In the presence of the different physics and time-scales, astronomers have mainly employed conserved quantities – energy and angular momentum – to roughly model CEE. These are known as the energy formalism (Webbink 1984) and the angular momentum (or γ) formalism (Nelemans et al. 2000). Because of the uncertainties in theoretical modeling of CEE, we bring numerical tools to bear. To perform 3-D simulations of CEE, two main approaches are used. The first is smoothed-particle hydrodynamics (SPH), where fluid quantities are determined from a finite sampling of nearby particles. SPH is computationally inexpensive and obeys conservation laws well, but the smoothing means that it has difficulty in handling discontinuities (i.e. shock waves). The other approach is Eulerian grid-based solvers, which are superior at capturing shocks but suffer from grid effects and violation of conservation laws (Springel 2010). The defining numerical studies are those carried out by Passy et al. (2012), Ricker & Taam (2012) and Nandez et al. (2015). Nandez et al. (2015) use a SPH code, Passy et al. (2012) use both a SPH and an Eulerian code and Ricker & Taam (2012) use an adaptive mesh refinement Eulerian code.

In recent years, a hybrid of these methods has been developed in an attempt to capture the best characteristics of both. This is the arbitrary Lagrangian-Eulerian (ALE) scheme, and software that use ALE schemes are known as moving-mesh codes. In an ALE scheme, the mesh moves along with the fluid, combining the superior shock-capturing of

[*] The author is supported by the R1 Distinguished Dissertation Fellowship at UWM and by the NASA Astrophysical Theory Program (ATP) through NASA grant NNH17ZDA001N-ATP. We use the Extreme Science and Engineering Discovery Environment (XSEDE), which is supported by National Science Foundation (NSF) grant No. ACI-1053575. We acknowledge the Texas Advanced Computing Center (TACC) at The University of Texas at Austin for providing HPC resources that have contributed to the research results reported within this paper (URL: http://www.tacc.utexas.edu). Computational resources supporting this work were also provided by the NASA High-End Computing (HEC) Program through the NASA Advanced Supercomputing (NAS) Division at the Ames Research Center. This material is based upon work supported by NASA under Award No. RFP21_7.0 issued through the Wisconsin Space Grant Consortium and the National Space Grant College and Fellowship Program. Any opinions, findings and conclusions or recommendations expressed in this material are those of the author and do not necessarily reflect the views of the National Aeronautics and Space Administration. We thank Philip Chang for useful and detailed discussions.

grid-based solvers with the conservation properties of SPH. Springel (2010) described one such scheme that has proven successful, which is implemented in the code AREPO. The scheme constructs an unstructured mesh from an arbitrary distribution of points using a Voronoi tessellation. This guarantees that the mesh will be well-defined, unique and continuously deformable; thus, finite-volume methods can be applied in a manner similar to that of an Eulerian code. In addition, the lack of Galilean invariance in Eulerian codes is rectified if the mesh cells move along with the local flow. A moving-mesh hydrodynamic solver has also been developed for the N-body simulation code ChaNGa (Charm N-body GrAvity solver) (Jetley et al. 2008, 2010; Menon et al. 2015). This moving-mesh solver is known as MANGA, which is is described in detail by Chang et al. (2017). In Prust & Chang (2019, hereinafter PC19), we incorporated individual time-steps into MANGA and showed that this results in a speedup of a factor of 4 to 5 for a CEE simulation.

Numerical simulations by a number of previous groups (Passy et al. 2012, for example) have found that only 5% to 25% of the envelope is ejected during CEE. This differs from the large implied values of ejection efficiency from observational studies, which suggests the existence of some additional energy not accounted for in the simulations. This changed with the SPH simulation of Nandez et al. (2015), who found that including hydrogen recombination energy leads to a complete ejection of the envelope and the formation of a clean double white dwarf binary. Indeed, we found in PC19 that the inclusion of hydrogen recombination has a large effect on envelope ejection. However, this point is controversial, as Soker and collaborators have claimed in a series of papers (Sabach et al. 2017, for example) that the energy from recombination is transported away either by radiation or convection and does not contribute to envelope ejection. This suggests that the incorporation of radiation physics may be an important next step in modeling CEE.

Recently, a module has been added to MANGA that solves the equations of time-dependent radiative transfer using a reduced speed of light approximation (Chang et al. 2020), following the algorithm of Jiang et al. (2014). Specific radiative intensities are solved along discrete angles, and can be integrated to find energy and momentum source terms. The radiation is coupled to the fluid by including these source terms in the hydrodynamic equations. This differs from moment formalisms such as M1 and flux-limited diffusion, which introduce closure relations to solve the radiative transfer equations (González et al. 2007). Because of the high opacity near the center of giant stars, the inclusion of radiation limits the time-step to a small value. Thus, we sub-cycle the radiation such that it is evolved for several time-steps for each single step of the fluid as in Kannan et al. (2019).

We have organized this paper as follows. In section 2, we summarize the algorithm of MANGA as well as the radiation hydrodynamics solvers. We then outline our implementation of radiation sub-cycling into MANGA in section 3. Section 4 delves into the generation of initial conditions for our simulations, and the results are covered in section 5. We conclude and discuss future directions in section 6.

2. MANGA Algorithm

The ALE algorithm that is implemented in MANGA is briefly summarized as follows. We refer the reader to Chang et al. (2017) and PC19 for detailed discussions. MANGA solves the Euler equations, which written in conservative form are

$$\frac{\partial \rho}{\partial t} + \boldsymbol{\nabla} \cdot \rho \boldsymbol{v} = 0, \tag{1}$$

$$\frac{\partial \rho \boldsymbol{v}}{\partial t} + \boldsymbol{\nabla} \cdot \rho \boldsymbol{v}\boldsymbol{v} + \boldsymbol{\nabla} P = -\rho \boldsymbol{\nabla} \Phi \tag{2}$$

and

$$\frac{\partial \rho e}{\partial t} + \boldsymbol{\nabla} \cdot (\rho e + P)\, \boldsymbol{v} = -\rho \boldsymbol{v} \cdot \boldsymbol{\nabla} \Phi, \tag{3}$$

where ρ is the density, $\boldsymbol{v}$ is the fluid velocity, Φ is the gravitational potential, $e = \epsilon + v^2/2$ is the specific energy, ϵ is the internal energy and $P(\rho, \epsilon)$ is the pressure. Eq. 1 to 3 can be written in a compact form by introducing a state vector $\boldsymbol{\mathcal{U}} = (\rho, \rho\boldsymbol{v}, \rho e)$:

$$\frac{\partial \boldsymbol{\mathcal{U}}}{\partial t} + \boldsymbol{\nabla} \cdot \boldsymbol{\mathcal{F}} = \boldsymbol{\mathcal{S}}, \tag{4}$$

where $\boldsymbol{\mathcal{F}} = (\rho \boldsymbol{v}, \rho \boldsymbol{v}\boldsymbol{v} + P, (\rho e + P)\boldsymbol{v})$ is the flux function and $\boldsymbol{\mathcal{S}} = (0, -\rho \boldsymbol{\nabla}\Phi, -\rho \boldsymbol{v} \cdot \boldsymbol{\nabla}\Phi)$ is the source function. To solve Eq. 4, we adopt the same finite-volume strategy as Springel (2010). For each cell, the integral over the volume of the ith cell V_i defines the charge of the ith cell to be

$$\boldsymbol{U}_i = \int_{V_i} \boldsymbol{\mathcal{U}} dV = \boldsymbol{\mathcal{U}}_i V_i. \tag{5}$$

We then use Gauss' theorem to convert the volume integral over the divergence of the flux in Eq. 4 to a surface integral

$$\int_{\partial V_i} \boldsymbol{\nabla} \cdot \boldsymbol{\mathcal{F}} dV = \int_{\partial V_i} \boldsymbol{\mathcal{F}} \cdot \hat{\boldsymbol{n}} dA, \tag{6}$$

where ∂V_i is the boundary of the cell. We now take advantage of the fact that the volumes are Voronoi cells with a finite number of neighbours to define an integrated flux

$$\sum_{j \in \text{neighbors}} \boldsymbol{F}_{ij} A_{ij} = \int_{\partial V_i} \boldsymbol{\mathcal{F}} \cdot \hat{\boldsymbol{n}} dA, \tag{7}$$

where $\boldsymbol{F}_{ij}$ and A_{ij} are the average flux and area of the common face between cells i and j. The discrete time evolution of the charges in the system is given by

$$\boldsymbol{U}_i^{n+1} = \boldsymbol{U}_i^n + \Delta t \sum_j \hat{\boldsymbol{F}}_{ij} A_{ij} + \Delta t \boldsymbol{S}_i, \tag{8}$$

where $\hat{\boldsymbol{F}}_{ij}$ is an estimate of the half time-step flux between the initial $\boldsymbol{U}_i^n$ and final states $\boldsymbol{U}_i^{n+1}$ and $\boldsymbol{S}_i^{(n+1/2)} = \int_i \boldsymbol{\mathcal{S}} dV$ is the time-averaged integrated source function.

When radiation is included, another conservation equation is needed to solve the time evolution of the radiation:

$$\frac{\partial I}{\partial t} + \bar{c}\hat{\boldsymbol{n}}_r \cdot \nabla I = \bar{c}\rho(\kappa_{\mathrm{P}} \frac{aT^4}{4\pi} + \kappa_{\mathrm{S}} \frac{1}{4\pi} \int I d\Omega - (\kappa_{\mathrm{J}} + \kappa_{\mathrm{S}})I). \tag{9}$$

Here I is the radiation intensity, $\hat{\boldsymbol{n}}_r$ is a normal vector, ρ is the gas density, and κ_{P}, κ_{S}, and κ_{J} are opacities. Finally, $\bar{c}$ is known as the reduced speed of light. MANGA uses the reduced speed of light approximation, meaning that we choose a value for the speed of light that is lower than the standard speed of light in a vacuum c. This aids in computation time and code stability, and is a valid approximation provided that $\bar{c}$ is at least several times larger than the largest fluid velocity present in the system.

The radiation interacts with the fluid by introducing source terms into the momentum equation 2 and energy equation 3. To this end, the first and second moments of the intensity

$$J = \frac{1}{4\pi} \int I d\Omega \quad \text{and} \quad \boldsymbol{H} = \frac{1}{4\pi} \int \hat{\boldsymbol{n}}_r I d\Omega \tag{10}$$

are used to compute the energy density and radiation flux tensors

$$E_r = \frac{4\pi}{c} J \quad \text{and} \quad \boldsymbol{F}_r = 4\pi \boldsymbol{H}. \tag{11}$$

The source terms are then constructed using E_r and $\boldsymbol{F}_r$ along with weights W_i corresponding to the specific angles along which the intensity is solved.

Finally, we take radiation into account during the flux computations to determine the amount of radiation advected across the face separating one cell from another. Because MANGA is a moving-mesh code, this requires us to take into account the velocity of the face $\boldsymbol{v}_{\text{face}}$. The flux is then

$$\boldsymbol{\mathcal{F}} = (\bar{c}\hat{\boldsymbol{n}}_r - \boldsymbol{v}_{\text{face}})I. \tag{12}$$

The radiative intensity I used for this calculation is that of the cell *upwind* of the face (the cell that the face is moving toward).

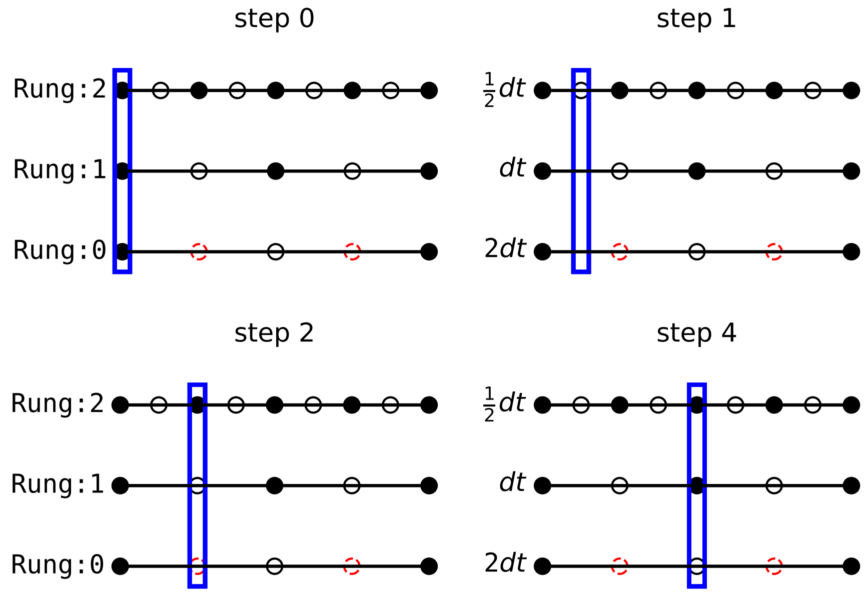

Figure 1: Integration of time-stepping for individual time-steps. Starting at the lowest rung (rung 0), the time-step is decreased by 2 for each higher rung. Full and half time-steps at each rung are shown as solid and empty circles, respectively. The time-stepper (blue rectangle) steps at the smallest half time-step, which in this case is at $0.25\delta t$. All particles drift along at this smallest time-step following the time-stepper. Half time-step procedures (full time-step Riemann solutions on half time-step Voronoi cells) are executed only at half time-steps relevant to the particular rung level. Full time-step procedures (accumulating all $\delta\boldsymbol{U}$'s and full time-step gradients and half time-step prediction) are executed at full time-steps. Note that only one half time-step at one rung is relevant for each step of the time-stepper, but multiple full time-steps at more than one rung can be executed at the time-stepper's current position.

3. Radiation Sub-Cycling

In the hot interior regions of stars, the inclusion of radiation can limit the time-step to a prohibitively small value. This is alleviated somewhat by the individual time-stepping algorithm implemented in PC19, though the presence of radiation also lowers the time-step throughout the rest of the simulation box to varying degrees. To combat this, we have implemented radiation sub-cycling into MANGA so that the equations of radiative transfer are evolved on a time-step separate from that used for the hydrodynamics, gravity, and mesh computations. This allows us to skip calculations that are unnecessary and often expensive, particularly regarding the Voronoi mesh generation.

To understand the sub-cycling implementation, it is first necessary to discuss the individual time-stepping algorithm, which we summarize here. We direct the interested reader to PC19 for a detailed discussion. The basic (universal) time-stepping algorithm for a second-order accurate (in time) integrator can be broken down into 3 stages: the initial time (a), the half time-step (b) and the full time-step (c) (Fig. 1).

(a) *Initial time* $t = 0$: determine Voronoi cells using current positions of mesh-generating points. Estimate gradients and construct half time-step predictions. Zero out the changes to the charges, e.g., $\delta \boldsymbol{U} = 0$.

(b) *Half time-step* $t = 0.5\delta t$: drift Voronoi cells to half time-step positions. Construct Voronoi cells at half time-steps. Compute the gradients and perform linear reconstruction to the half time-step cell faces to compute fluxes. Perform a Riemann solution and incorporate source terms with the *full* time-step. Place these changes into $\delta \boldsymbol{U}$.

(c) *Full time-step* $t = \delta t$: drift Voronoi cells to full time-step positions. Advance charges to be $\boldsymbol{U}^{n+1} = \boldsymbol{U}^n + \delta \boldsymbol{U}$. Reset the state to be the new initial time.

We note that the full time-step for any cell involves actions at a full time-step (a,c) and the half time-step (b). For individual time-steps, we assign to each particle a time-step level which we refer to as a "rung," where each rung has a smaller time-step than the rung below it by a factor of two. Therefore, at the half time-step for some rung i, full time-steps are executed for all rungs $j > i$. Cells are allowed to change rungs only at their full time-steps. Additionally, we limit the time-step of any cell to be less than $\sqrt{2}$ of the minimum time-step of its neighbors. This ensures that the time-step changes by no more than a factor of 2 (and the rung by no more than 1) over a distance of two cells. This is similar to the time-step smoothing over a SPH kernel used by Saitoh & Makino (2009), and we find that it allows for stable integrations in MANGA. PC19 finds that individual time-stepping decreases the computation time by a factor of 4 to 5 for a CEE simulation.

The same method of assigning rungs is used when radiation is present. However, rather than assigning a particle to a single rung, it is assigned two rungs: one for radiation, and one for everything else. Because the speed of light is involved in the rung calculation, the radiation rung is higher (corresponding to a smaller time-step) for the vast majority of particles. For example, if a particle is on rung 2 but has a radiation rung of 5, this means that the radiation time-step is a factor of $2^{(5-2)} = 8$ smaller than that of all other time-step constraints, and that 8 radiation steps will be performed for each single step of the hydrodynamics, gravity, and mesh. This is because when the time-stepper reaches rungs 3, 4, and 5, only the radiation solvers will be called for that particle. MANGA also has the capability to manually set the number of radiation steps per hydrodynamic step – as is done in Kannan et al. (2019) – but this method can lead to violations of the Courant time-step condition and does not necessarily reduce computation time.

We have also worked to reduce inefficiencies in the overall structure of the code by removing redundant mesh calculations. For instance, we have eliminated the calculation of the shapes of the Voronoi cells at the beginning of each time-step, instead using the results for the same calculation performed at the end of the previous step. Additionally, each cell must search over the surrounding cells to determine with which of its neighbors it shares a face, which can be an expensive process. We have determined several instances in which nearest neighbor maps can be reused to avoid redoing this search. The speedups provided by these optimizations as well as the sub-cycling depend on the specific nature of the simulation, but in general we find a factor of 2 speedup from sub-cycling and 1.5 from mesh optimizations. Thus, we have decreased the total computation time by a factor of $\sim$3.

4. Simulation Setup

We now outline the development of appropriate initial conditions for CEE simulations in MANGA. The reader is referred to PC19 for a detailed discussion. We first use the open-source stellar evolution code MESA (Paxton et al. 2011, 2013, 2015, 2018, 2019) to evolve a 2 $\mathrm{M}_\odot$ star with metallicity $Z = 0.02$ from the pre-main sequence to the red giant phase. We stop when the star reaches 52 $\mathrm{R}_\odot$ with a helium core mass of 0.36 $\mathrm{M}_\odot$. From the MESA output, we take the entropy and hydrogen fraction. For the core, we take the total mass at a density that is 50 times greater than the mean density of the red giant, giving a core mass $M_\mathrm{c} = 0.379\ \mathrm{M}_\odot$. This corresponds to a core radius $R_\mathrm{c} = 1.99\ \mathrm{R}_\odot$, which we use as the core gravitational softening length h. For all particles present regardless of type, MANGA uses spline softening to soften the gravitational forces within radius h of the particle. Because of the great difference in density between the helium core and the hydrogen envelope, we model the core as a dark matter particle with mass M_c and softening radius of R_c. We then take the entropy profile and construct a star of mass $M - M_\mathrm{c}$, with an entropy profile which matches that of the original star and contains a dark matter particle core. This yields a radial profile of density, temperature and hydrogen fraction that can be mapped to a particle (mesh-generating point) profile.

We construct an appropriate particle mesh for the star from a pre-computed glass distribution of points embedded in a 3-D cube. We periodically replicate this glass distribution to produce a sufficient number of particles. We assume that each particle is of equal volume and rescale them to the appropriate mass based on the computed $M(r)$ from MESA. These particles are also endowed with the radially interpolated temperature and hydrogen fraction. The total number of particles representing the star is 1.8×10^5. Outside of the star, we include a low density atmosphere of 10^{-13} g cm^{-3} with temperature 10^5 K that extends out to the total box size of 3.5×10^{14} cm (5000 $\mathrm{R}_\odot$), with periodic boundary conditions at its edges. The total number of particles in the simulation box is 1.1×10^6. To lower the computational cost, we use a mesh refinement algorithm to decrease the number of gas particles in the atmosphere far from the star. We define a scale factor $\mathcal{S}(r) = (r/R_*)^n$ where R_* is the radius of the star, r is the spherical radius and n is an adjustable parameter which we have set to $n = 3$ in this case. Starting with the same uniform glass distribution as for the star, the linear spacing between particles is increased by $\mathcal{S}$ and their mass is increased by $\mathcal{S}^3$, preserving the external density.

The radiation is initialized such that it is in local thermodynamic equilibrium with the gas. That is, the radiation is initially isotropic with intensity $I = aT_\mathrm{gas}^4/4\pi$, where T_gas is the local gas temperature.

We place the 1 $\mathrm{M}_\odot$ companion in an initially circular Keplerian orbit at the surface of the red giant ($a = 52\ \mathrm{R}_\odot$). Although this neglects the evolution of the binary prior to CEE, we compensate by altering the dynamics of the giant. We have implemented the corotation between the envelope rotation and orbital motion into our simulations following the scheme of MacLeod et al. (2018). Within the envelope, we assume rigid body rotation and initialize the velocity as

$$v_\phi = f_\mathrm{cr}\Omega_\mathrm{orb}R_\mathrm{cyl}, \tag{13}$$

but give the atmosphere a velocity

$$v_\phi = \frac{f_\mathrm{cr}\Omega_\mathrm{orb}R_*^2\sin^2(\theta)}{R_\mathrm{cyl}}. \tag{14}$$

Here, f_cr is an adjustable parameter which we have set to unity, ϕ is the azimuthal angle, θ is the polar angle, Ω_orb is the orbital frequency of the red giant and companion, R_* is the radius of the giant and R_cyl is the cylindrical radius from the rotation axis of the giant. We note that Eq. 13 and 14 ensure that the velocity is continuous at the surface of the giant.

5. Results

We carry out a simulation of CEE using the above initial conditions. However, we have encountered a roadblock for performing these runs. At the start of a CEE phase, the large density gradients inside of the red giant can cause errors in the radiation solvers. One possible work-around that we devised is to run the early stages of the simulation without radiation and to turn it on once these gradients have dissipated. This should not pose a threat to the validity of the results, as radiation is thought to be significant only at late times. The reasoning is as follows: hydrogen recombination can only occur after gas has been thrown off of the red giant and has had enough time to cool, and radiation is only significant after recombination has occurred. Although we have been successful in turning on radiation within our simulations, significant density gradients persist for much longer than expected. To avoid crashes, we are forced to make unphysical choices for either the gas opacity or the reduced speed of light. Since both of these quantities affect the interactions between radiation and matter, we have not been able to attain any believable simulation results. For this reason, the simulation here is presented without radiation.

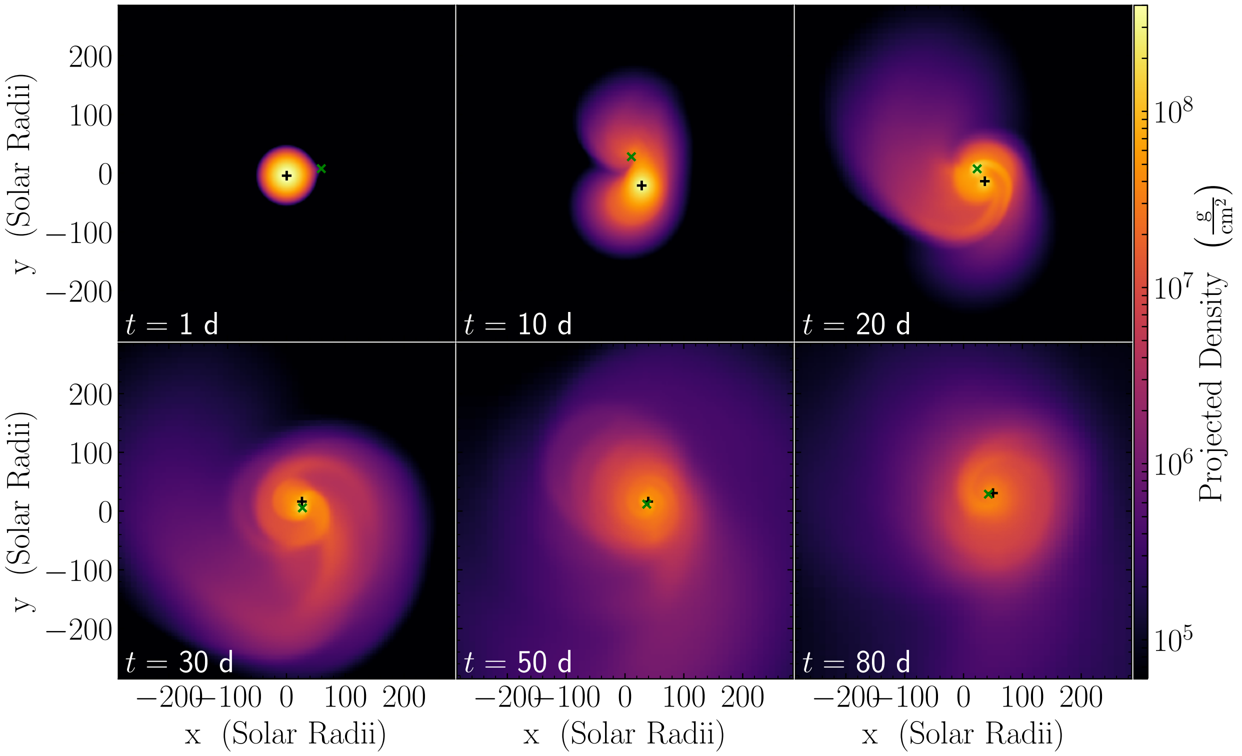

Figure 2: Density projections in our CEE simulation. The + sign marks the red giant core and the × marks the companion.

We show density projections at $t = 1$, 10, 20, 30, 50 and 80 days in Fig. 2. The companion experiences an initial plunge into the envelope of the giant that lasts about 18 days, throwing off a large tidal tail and greatly decreasing the separation between the companion and core. The companion then continues to spiral in as its orbital energy is transferred to the gas; the spiral shocks facilitating this transfer can be seen in the projections (Fig. 2 upper right and lower left). The simulation ends well before the outflows reach the edge of the simulation box. The separation between the stellar core and companion is shown in Fig. 3. After one orbit, the binary has reduced its orbital separation to less than half the initial separation, and continues to spiral in at a slower rate. This is the behavior expected of a common envelope phase, and it is worthwhile to verify that the results are accurate prior to the inclusion of radiation physics.

6. Discussion

In this paper we have attempted to use the recently-developed radiation hydrodynamics module in MANGA to simulate CEE in binary stars. It is known that the inclusion of hydrogen recombination energy has a large effect on the outcome of CEE, but it is not clear how much of this energy is available to assist in envelope ejection and how much is radiated away. Thus, the use of radiation hydrodynamics is an important next step in this investigation. We have summarized the radiation solvers, which introduce a new conservation equation describing the radiation intensity and introduce new source terms in the momentum and energy equations. An upwind solver is also used for the flux calculations to determine the flow of radiation across the faces.

A new radiation sub-cycling algorithm has been implemented to combat the small time-steps that can be encountered

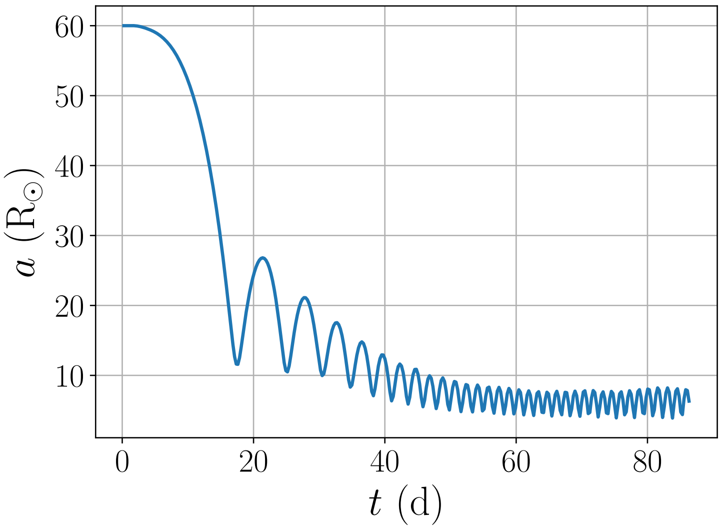

Figure 3: Separation a between the stellar core and companion.

when radiation is present. These small time-steps are due in large part to the inclusion of the speed of light in the time-step calculations, even with the use of the reduced speed of light approximation. It is therefore desirable to evolve the radiation on a different time-step than that of the hydrodynamic, gravity, and mesh calculations. This avoids unnecessary and expensive calculations, especially in the case of the Voronoi mesh generation. We improve on the method of Kannan et al. (2019), which manually set the number of radiation steps per hydrodynamic step, by allowing each particle to individually determine the appropriate rung for each type of solver. The sub-cycling as well as the reduction of inefficiencies in the mesh generation have led to a reduction in computation time by a factor of 3.

Initial conditions for CEE simulations of a 2 M$_\odot$ red giant with a 1 M$_\odot$ companion were also described, largely following PC19. We have also included initial conditions for the radiation intensity so that the radiation is – at least initially – in thermodynamic equilibrium with the gas.

Due to errors in the code caused by the large density gradients present in red giants, we have been unable to perform a stable integration of CEE with radiation present. Delaying the inclusion of radiation until a later time within the simulation has been attempted, but the problem persists even to late times. The code is stable provided that either the gas opacity or the reduced speed of light are taken to be very small, though this is unphysical and any results obtained from such simulations would not be useful. Thus, we have shown a run without radiation that shows the expected features of a common envelope phase.

One promising solution to these issues is the implicit solver recently proposed in Jiang (2021), which is implemented in the Athena++ code. This would allow for stable solutions even in the optically thick centers of stars and would use the standard (rather than reduced) speed of light. It would also remove any time-step constraint related to the speed of light, which would further reduce computation time. Though this would be a substantial code development project, we plan to go forward with implementing it into MANGA.

Acknowledgments

We thank Philip Chang for useful and detailed discussions. We are supported by the R1 Distinguished Dissertation Fellowship at UWM and by the NASA Astrophysical Theory Program (ATP) through NASA grant NNH17ZDA001N-ATP. We use the Extreme Science and Engineering Discovery Environment (XSEDE), which is supported by National Science Foundation (NSF) grant No. ACI-1053575. We acknowledge the Texas Advanced Computing Center (TACC) at The University of Texas at Austin for providing HPC resources that have contributed to the research results reported within this paper (URL: http://www.tacc.utexas.edu). We use the YT software platform for the analysis of the data and generation of plots in this work (Turk et al. 2011). Computational resources supporting this work were also provided by the NASA High-End Computing (HEC) Program through the NASA Advanced Supercomputing (NAS) Division at the Ames Research Center. This material is based upon work supported by NASA under Award No. RFP21_7.0 issued through the Wisconsin Space Grant Consortium and the National Space Grant College and Fellowship Program. Any opinions, findings and conclusions or recommendations expressed in this material are those of the author and do not necessarily reflect the views of the National Aeronautics and Space Administration.

References

Chang, P; Davis, SW; Jiang, YF. “Time-dependent radiation hydrodynamics on a moving mesh,” *MNRAS*, v. 493(4), 2020, p. 5397–5407. https://ui.adsabs.harvard.edu/abs/2020MNRAS.493.5397C

Chang, P; Wadsley, J; Quinn, T. “A Moving Mesh Hydrodynamics Solver for ChaNGa,” *accepted to MNRAS*, 2017

González, M; Audit, E; Huynh, P. “HERACLES: a three-dimensional radiation hydrodynamics code,” *A&A*, v. 464(2), 2007, p. 429–435. https://ui.adsabs.harvard.edu/abs/2007AA...464..429G

Ivanova, N; Justham, S; Chen, X; De Marco, O; Fryer, CL; Gaburov, E; Ge, H; Glebbeek, E; Han, Z; Li, XD; Lu, G; Marsh, T; Podsiadlowski, P; Potter, A; Soker, N; Taam, R; Tauris, TM; van den Heuvel, EPJ; Webbink, RF. “Common envelope evolution: where we stand and how we can move forward,” *A&A Rev.*, v. 21, 2013, p. 59. http://ukads.nottingham.ac.uk/abs/2013A%26ARv..21...59I

Jetley, P; Gioachin, F; Mendes, C; Kale, LV; Quinn, TR. “”massively parallel cosmological simulations with changa”,” *Proceedings of IEEE International Parallel and Distributed Processing Symposium*, 2008

Jetley, P; Wesolowski, F; Gioachin, F; Kale, LV; Quinn, TR. “”scaling hierarchical n-body simulations on gpu clusters”,” *Proceedings of the 2010 ACM/IEEE International Conference for High Performance Computing*, 2010

Jiang, YF. “An Implicit Finite Volume Scheme to Solve the Time-dependent Radiation Transport Equation Based on Discrete Ordinates,” *ApJS*, v. 253(2), 2021, p. 49. https://ui.adsabs.harvard.edu/abs/2021ApJS..253...49J

Jiang, YF; Stone, JM; Davis, SW. “An Algorithm for Radiation Magnetohydrodynamics Based on Solving the Time-dependent Transfer Equation,” *ApJS*, v. 213(1), 2014, p. 7. https://ui.adsabs.harvard.edu/abs/2014ApJS..213....7J

Kannan, R; Vogelsberger, M; Marinacci, F; McKinnon, R; Pakmor, R; Springel, V. “AREPO-RT: radiation hydrodynamics on a moving mesh,” *MNRAS*, v. 485(1), 2019, p. 117–149. https://ui.adsabs.harvard.edu/abs/2019MNRAS.485..117K

MacLeod, M; Ostriker, EC; Stone, JM. “Runaway Coalescence at the Onset of Common Envelope Episodes,” *ApJ*, v. 863, 2018, p. 5. https://ui.adsabs.harvard.edu/#abs/2018ApJ...863....5M

Menon, H; Wesolowski, L; Zheng, G; Jetley, P; Kale, L; Quinn, T; Governato, F. “Adaptive techniques for clustered N-body cosmological simulations,” *Computational Astrophysics and Cosmology*, v. 2, 2015, p. 1. http://adsabs.harvard.edu/abs/2015ComAC...2....1M

Nandez, JLA; Ivanova, N; Lombardi, JC. “Recombination energy in double white dwarf formation,” *MNRAS*, v. 450, 2015, p. L39–L43. http://adsabs.harvard.edu/abs/2015MNRAS.450L..39N

Nelemans, G; Verbunt, F; Yungelson, LR; Portegies Zwart, SF. “Reconstructing the evolution of double helium white dwarfs: envelope loss without spiral-in,” *A&A*, v. 360, 2000, p. 1011–1018. http://adsabs.harvard.edu/abs/2000A%26A...360.1011N

Passy, JC; De Marco, O; Fryer, CL; Herwig, F; Diehl, S; Oishi, JS; Mac Low, MM; Bryan, GL; Rockefeller, G. “Simulating the Common Envelope Phase of a Red Giant Using Smoothed-particle Hydrodynamics and Uniform-grid Codes,” *ApJ*, v. 744, 2012, p. 52. http://adsabs.harvard.edu/abs/2012ApJ...744...52P

Paxton, B; Bildsten, L; Dotter, A; Herwig, F; Lesaffre, P; Timmes, F. “Modules for Experiments in Stellar Astrophysics (MESA),” *ApJS*, v. 192, 2011, p. 3. http://adsabs.harvard.edu/abs/2011ApJS..192....3P

Paxton, B; Cantiello, M; Arras, P; Bildsten, L; Brown, EF; Dotter, A; Mankovich, C; Montgomery, MH; Stello, D; Timmes, FX; Townsend, R. “Modules for Experiments in Stellar Astrophysics (MESA): Planets, Oscillations, Rotation, and Massive Stars,” *ApJS*, v. 208, 2013, p. 4. http://adsabs.harvard.edu/abs/2013ApJS..208....4P

Paxton, B; Marchant, P; Schwab, J; Bauer, EB; Bildsten, L; Cantiello, M; Dessart, L; Farmer, R; Hu, H; Langer, N; Townsend, RHD; Townsley, DM; Timmes, FX. “Modules for Experiments in Stellar Astrophysics (MESA): Binaries, Pulsations, and Explosions,” *ApJS*, v. 220, 2015, p. 15. http://adsabs.harvard.edu/abs/2015ApJS..220...15P

Paxton, B; Schwab, J; Bauer, EB; Bildsten, L; Blinnikov, S; Duffell, P; Farmer, R; Goldberg, JA; Marchant, P; Sorokina, E; Thoul, A; Townsend, RHD; Timmes, FX. “Modules for Experiments in Stellar Astrophysics (MESA): Convective Boundaries, Element Diffusion, and Massive Star Explosions,” *ApJS*, v. 234(2), 2018, p. 34. https://ui.adsabs.harvard.edu/abs/2018ApJS..234...34P

Paxton, B; Smolec, R; Schwab, J; Gautschy, A; Bildsten, L; Cantiello, M; Dotter, A; Farmer, R; Goldberg, JA; Jermyn, AS; Kanbur, SM; Marchant, P; Thoul, A; Townsend, RHD; Wolf, WM; Zhang, M; Timmes, FX. “Modules for Experiments in Stellar Astrophysics (MESA): Pulsating Variable Stars, Rotation, Convective Boundaries, and Energy Conservation,” *ApJS*, v. 243(1), 2019, p. 10. https://ui.adsabs.harvard.edu/abs/2019ApJS..243...10P

Prust, LJ; Chang, P. “Common envelope evolution on a moving mesh,” *MNRAS*, v. 486(4), 2019, p. 5809–5818. https://ui.adsabs.harvard.edu/abs/2019MNRAS.486.5809P

Ricker, PM; Taam, RE. “An AMR Study of the Common-envelope Phase of Binary Evolution,” *ApJ*, v. 746, 2012, p. 74. http://adsabs.harvard.edu/abs/2012ApJ...746...74R

Sabach, E; Hillel, S; Schreier, R; Soker, N. “Energy transport by convection in the common envelope evolution,” *MNRAS*, v. 472, 2017, p. 4361–4367. https://ui.adsabs.harvard.edu/abs/2017MNRAS.472.4361S

Saitoh, TR; Makino, J. “A Necessary Condition for Individual Time Steps in SPH Simulations,” *ApJ*, v. 697, 2009, p. L99–L102. http://adsabs.harvard.edu/abs/2009ApJ...697L..99S

Springel, V. “E pur si muove: Galilean-invariant cosmological hydrodynamical simulations on a moving mesh,” *MNRAS*, v. 401, 2010, p. 791–851. http://adsabs.harvard.edu/abs/2010MNRAS.401..791S

Turk, MJ; Smith, BD; Oishi, JS; Skory, S; Skillman, SW; Abel, T; Norman, ML. “yt: A Multi-code Analysis Toolkit for Astrophysical Simulation Data,” *The Astrophysical Journal Supplement Series*, v. 192, 2011, p. 9. http://adsabs.harvard.edu/abs/2011ApJS..192....9T

Webbink, RF. “Double white dwarfs as progenitors of R Coronae Borealis stars and Type I supernovae,” *ApJ*, v. 277, 1984, p. 355–360. http://adsabs.harvard.edu/abs/1984ApJ...277..355W